Journal of Zhejiang University-SCIENCE A 2026 27(9):969-989
www.jzus.zju.edu.cn; www.springer.com/journal/11582
E-mail: jzus_a@zju.edu.cn

Review

https://doi.org/10.1631/jzus.A2600283

Check for updates

Deep-blue perovskite light-emitting diodes: towards high-performance and lead-free devices

Zhuoyue GU[1,2*], Zhengyang JU[1,2*], Kecong REN[1,2], Feiyang ZHANG[1,2], Shuailiang SHEN[1,2], Dawei DI[1,2,3✉], Baodan ZHAO[1,2✉]

[1]*State Key Laboratory of Extreme Photonics and Instrumentation, College of Optical Science and Engineering, Zhejiang University, Hangzhou 310027, China*
[2]*International Research Center for Advanced Photonics, Zhejiang University, Hangzhou 310027, China*
[3]*Zhejiang University-University of Illinois Urbana-Champaign Institute, Zhejiang University, Jiaxing 314400, China*

Abstract: Perovskite light-emitting diodes (PeLEDs) have emerged as a prominent research direction in optoelectronic devices due to their unique advantages. However, deep-blue PeLEDs still exhibit a significant performance gap compared to their red and green counterparts. This review summarizes the current primary approaches for optimizing the performance of deep-blue PeLEDs. Doping with halogen elements and metal ions represents the mainstream strategy for achieving a blue shift in the emission wavelength. Optimization of fabrication processes enables improved luminescence performance through morphological and dimensional control. We also discuss the current research status of lead-free deep-blue PeLEDs and compare the performance between lead-free and lead-containing devices. Finally, we provide perspectives on future research and industrial development directions for deep-blue PeLEDs.

Key words: Deep-blue emitting; Perovskite; Light-emitting diode (LED); Lead-free

1 Introduction

Since the first report of room-temperature electroluminescence (EL) in halide perovskite, perovskite light-emitting diodes (PeLEDs) have rapidly emerged as a research hotspot in the fields of display and lighting due to their unique advantages (Tan et al., 2014). With their tunable bandgaps, high color purity, and low-cost solution processability, PeLEDs hold great promise for a wide range of emerging applications (Zhao et al., 2023). For next-generation display technology, they are suitable light sources for the International Telecommunication Union-Radiocommunication Sector (ITU-R) Recommendation BT.2020 (Rec. 2020) color gamut, enabling wider color triangles for ultra-high-definition displays. Additionally, PeLEDs are promising candidates for circularly polarized emitters in 3D displays, virtual reality (VR), and augmented reality (AR) devices. In particular, with amplified spontaneous emission in metal halide perovskites, deep-blue PeLEDs are considered excellent candidates for electrically pumped lasers, leveraging their high carrier mobility and high photoluminescence quantum yield (PLQY) (Xing et al., 2014).

However, despite significant progress in green and red PeLEDs with external quantum efficiencies (EQEs) exceeding 30% (Feng et al., 2024; Li MM et al., 2024; Jiang et al., 2025), the development of deep-blue devices that meet the Rec. 2020 (Commission Internationale de l'Éclairage (CIE) coordinates (0.131, 0.046); emission wavelength ⩽465 nm) lags considerably (Han et al., 2022). This pronounced "color imbalance" hinders full-color display industrialization (Ko et al., 2025). Although recent years have witnessed significant performance improvements in deep-blue PeLEDs, including a peak EQE of 15.4% at 459 nm through multivalent stabilization (Dong et al., 2025), these devices have consistently struggled to reach the EQE levels of green

✉ Dawei DI, daweidi@zju.edu.cn
Baodan ZHAO, baodanzhao@zju.edu.cn
* The two authors contributed equally to this work
Baodan ZHAO, https://orcid.org/0000-0002-4006-7061
Dawei DI, https://orcid.org/0000-0003-0703-2809

Received Apr. 30, 2026; Revision accepted July 10, 2026;
Crosschecked Aug. 19, 2026

and red PeLEDs. Furthermore, both the brightness and operational lifetime of deep-blue PeLEDs remain critically inadequate, falling far short of the requirements for commercial applications (Dong et al., 2025; Li et al., 2026).

In this review, we analyzed pathways for further enhancing the efficiency and stability of deep-blue PeLEDs. First, we outlined performance tuning strategies for lead-based deep-blue PeLEDs and summarize recent advancements. Second, we focused on research progress in lead-free deep-blue PeLEDs, discussing the structural characteristics, performance breakthroughs, and core challenges of this system (Fig. 1). Finally, we explored potential future research directions and industrialization pathways, including the pursuit of lead-free devices that simultaneously meet color standards, to advance deep-blue PeLEDs toward practical applications.

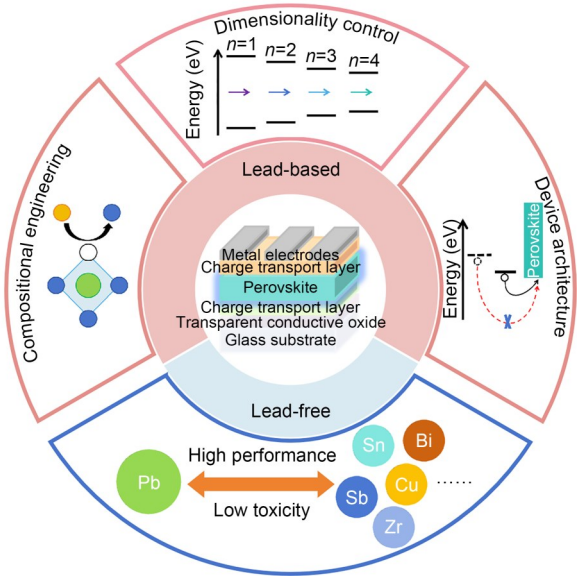

Fig. 1 Strategies for high performance in deep-blue PeLEDs and progress of lead-free devices

2 Deep-blue lead-based PeLEDs

PeLEDs typically adopt a multi-layer thin film stack structure, with core components including a transparent anode, a hole transport layer (HTL), a hole injection layer (HIL), a perovskite light-emitting layer, an electron transport layer (ETL), an electron injection layer, and a metal cathode. Under forward-bias driving, electrons and holes are injected from the cathode and anode, respectively, and migrate toward the central perovskite luminescent layer. Confined effectively within the luminescent layer, these carriers form excitons, which subsequently undergo radiative recombination to produce photons. EQE (E_{EQ}) is a key indicator for measuring the overall performance of this process:

$$E_{EQ}=f_{balance}\times f_{e-h}\times \eta_{rad}\times f_{outcoupling}, \quad (1)$$

where $f_{balance}$ is the factor of charge injection balance, f_{e-h} is the probability of producing a correlated electron–hole pair generated from each pair of injected carriers, η_{rad} is the radiative recombination efficiency of each electron–hole pair, and $f_{outcoupling}$ is the optical outcoupling efficiency (Zhao et al., 2023).

Specifically, for deep-blue PeLEDs, on the one hand, the emission of deep-blue light requires perovskite materials to have a large bandgap, which significantly increases the injection barrier of electrons and holes from the electrode to the emitting layer, making carrier injection very difficult. Meanwhile, wide bandgap materials often exhibit poor carrier mobility and higher defect state density, exacerbating non-radiative recombination losses. On the other hand, the deep-blue light band is close to the limit of human visual sensitivity, and the phase separation or spectral redshift phenomenon of large bandgap materials under the action of electric fields makes it difficult to maintain practical device efficiency, color stability, and lifetime (Ko et al., 2025).

2.1 Device optimization strategies

Achieving deep-blue lead-based PeLEDs compliant with the Rec. 2020 presents a significant challenge, as it requires precise wavelength control while simultaneously ensuring spectral stability and device performance. Obstacles such as halide segregation in mixed-halide perovskites, inefficient charge injection, and high defect densities hinder progress. To address these issues, this section discusses three key optimization strategies, including compositional engineering, size and dimensionality control, and device architecture optimization.

2.1.1 Compositional engineering

The bandgap of halide perovskite features high tunability, which can be achieved by changing its halide composition (Fig. 2a) (Protesescu et al., 2015). Br-Cl mixing is the key strategy for tuning the emission

properties of deep-blue PeLEDs. As halogens are mixed, the smaller Cl^- partially replaces Br^- within the perovskite lattice, leading to lattice contraction (Chen et al., 2021b). Additionally, as the halide composition shifts from I^- to Cl^-, enhanced orbital hybridization raises the conduction band level (Chen et al., 2021b). Consequently, the bandgap of the perovskite is modified, resulting in a blue shift of the emission wavelength.

However, increasing Cl content leads to unbalanced perovskite crystallization and limited solubility, which generates a high density of defects and reduces radiative recombination efficiency (Akkerman et al., 2015). The presence of halogen vacancy defects and phase segregation in mixed-halide perovskites poses significant challenges to achieving both target emission wavelengths and high efficiency (Fig. 2b) (Gao et al., 2024).

The vapor-assisted crystallization technique has been employed in the fabrication of perovskite films to mitigate ion migration and local heterogeneity (Karlsson et al., 2021). By treating the films in a dimethylformamide (DMF) atmosphere before annealing, a perovskite film with enhanced homogeneity and reduced defect density was obtained (Fig. 2c). The resulting device achieved an efficiency of 5.5% at an emission wavelength of 467 nm (Karlsson et al., 2021). Additive incorporation has also been used to achieve perovskite films with uniform halogen distribution. By introducing tetraphenylphosphonium bromide (TPPB) in combination with polyoxyethylene sorbitan monolaurate (Tween), the distribution homogeneity of Br and Cl in the perovskite precursor solution can be significantly enhanced (Cheng et al., 2020).

The in-situ halide exchange strategy has also been demonstrated as an effective method for modulating the halide ion ratios in perovskite films (Tong et al., 2023; Zeng et al., 2023; Zhang et al., 2024; Zhao SH et al., 2024). By spin-coating an organic ammonium halide salt containing Cl^-, such as tetraphenylphosphonium chloride (TPPC), onto the perovskite film, the excess Cl^- diffuses into the perovskite lattice, which effectively fills halide vacancies and partially substitutes bromide ions, thereby promoting a more uniform halogen distribution (Tong et al., 2023). However, the commonly used solvent for ammonium halide salts, isopropanol (IPA), tends to corrode the perovskite film and introduce defects (Fig. 2d) (Tong et al., 2023; Zhang et al., 2024). Conversely, the solubility of halide ammonium salts is excessively low in anti-solvents such as chloroform (CF) (Zeng et al., 2023; Zhao SH et al., 2024). Therefore, a nondestructive in-situ halide exchange strategy was developed using CF as an anti-solvent for post-treatment and long alkyl chain butylammonium halide salts as the Cl source, resulting in deep-blue PeLEDs with an EQE of 15% at 468 nm (Zhang et al., 2024).

Ion doping is another method to tune the emission bandgaps of perovskites. By doping smaller metal ions at the A-site or B-site of the perovskite, lattice deformation and contraction can be induced, thereby affecting the bandgap of the perovskite and modulating the emission wavelength (Gao et al., 2024). Alkali metal ions such as Rb^+ and K^+ are commonly used for A-site ion doping (Gao et al., 2024; Cao et al., 2025). The incorporation of relatively small Rb^+ ions at the A-site induces lattice contraction in the perovskite, which enhances the orbital overlap between lead and halide ions, thereby causing a blue shift in the emission wavelength. This method effectively reduced the Cl^- content in $CsPb(Br_xCl_{1-x})_3$ and, via Rb^+ compensation, further suppressed deep-level defect formation (Fig. 2e) (Gao et al., 2024). Substituting the B-site Pb^{2+} with smaller ions, such as Zn^{2+}, Cd^{2+}, and Sr^{2+}, represents another effective strategy for bandgap tuning (van der Stam et al., 2017; Chen Y et al., 2025). This doping-induced lattice contraction shortens the Pb-Br bond length, thereby enhancing the coupling between Pb and Br, which subsequently leads to a widened bandgap (van der Stam et al., 2017). While partial substitution of Pb^{2+} with Sn^{2+}, Cd^{2+}, or Zn^{2+} can induce a blue shift in the emission wavelength, it often results in a low PLQY (van der Stam et al., 2017). In contrast, the introduction of B-site Sr^{2+} doping promoted a more ordered arrangement at the A-site, optimized film crystallinity, and ultimately led to a PLQY of 75% (Fig. 2f) (Chen Y et al., 2025).

2.1.2 Size and dimensionality control

In the development of quantum dot (QD) and 2D/quasi-2D perovskite materials, the precise control of size and dimensionality is a key strategy for achieving efficient deep-blue emission. Through the quantum confinement effect, the energy level structure of QDs is closely related to their size, while low-dimensional perovskites modulate their electronic structure and luminescence properties by controlling the number of layers (*n*-value).

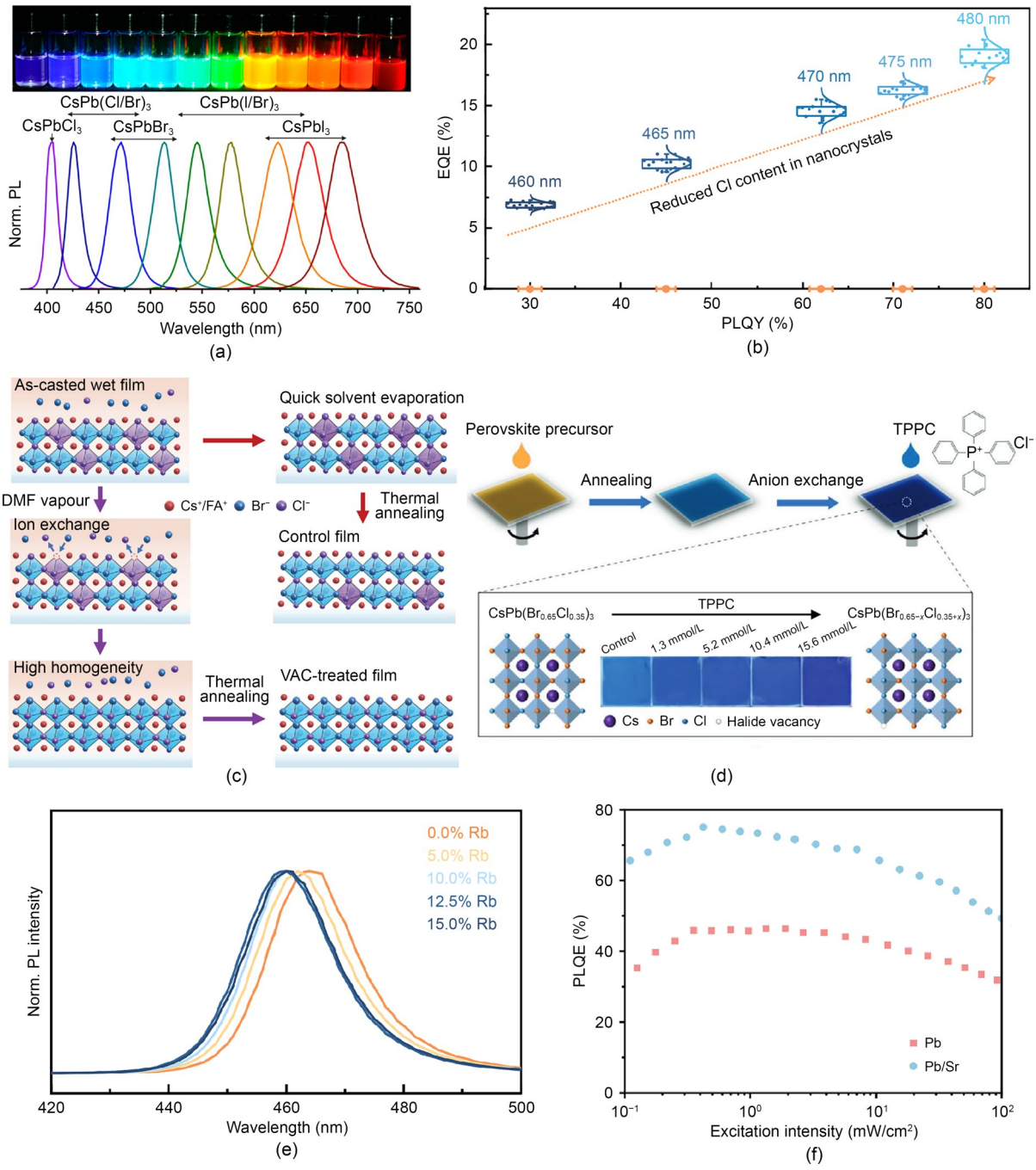

Fig. 2 (a) Colloidal perovskite $CsPbX_3$ (X=Cl, Br, and I) nanocrystals exhibiting size- and composition-tunable bandgap energies covering the entire visible spectral region with narrow and bright emission (Norm. PL is the normalized photoluminescence) (Protesescu et al., 2015); (b) statistical distributions of EQEs and average PLQYs varying with emission wavelength (the arrows represent the trends of reduced Cl content) (reprinted from (Gao et al., 2024), Copyright 2024, with permission from the American Association for the Advancement of Science); (c) schematic illustration of the mechanism of the vapor-assisted crystallization technique (FA is the formamidinium) (Karlsson et al., 2021); (d) schematic diagram of the in-situ halide exchange through treatments of organic halide salts on $CsPb(Br_{0.65}Cl_{0.35})_3$ perovskites (inset: photograph of the control perovskite treated by TPPC at various concentrations) (reprinted from (Tong et al., 2023), Copyright 2023, with permission from John Wiley and Sons); (e) finely tunable emission peak of $CsPb(Br_xCl_{1-x})_3$ nanocrystals with increasing levels of Rb incorporation (the PL spectra remain identical after a 10% feeding molar ratio of Rb to Cs) (reprinted from (Gao et al., 2024), Copyright 2024, with permission from the American Association for the Advancement of Science); (f) excitation-intensity-dependent PLQYs of B-site Sr^{2+} doping and pristine samples (Chen Y et al., 2025)

When the characteristic size of a nanoscale semiconductor material becomes comparable to the de Broglie wavelength of electrons in at least one dimension, quantum confinement effects restrict electrons within a confined spatial region. Consequently, the energy of the confined electrons assumes discrete values, corresponding to distinct energy levels. As zero-dimensional structures, QDs impose confinement on electrons in all three dimensions. The energy level spacing of the confined electrons is inversely correlated with the size of QDs: smaller QDs exhibit larger energy level spacing (Butkus et al., 2017). This relationship can be described by

$$\Delta E = \frac{\hbar^2 \pi^2}{2m^* r^2}, \tag{2}$$

where ΔE represents the energy level spacing of confined electrons in QDs, $\hbar$ represents the reduced Planck constant, r represents the particle radius, and m^* represents the effective mass of exciton (Butkus et al., 2017).

Compared to red and green PeLEDs, deep-blue QD PeLEDs require smaller QDs, which are typically achieved through methods such as halide composition adjustment, metal cation doping, and direct manipulation of the quantum confinement effect (Shan et al., 2024). A common method to reduce the size of QDs involves ligand-assisted replacement of Br^- with Cl^- in perovskites. However, the incorporation of Cl^- is frequently accompanied by the generation of deep-level defects (Zheng et al., 2020). Alternatively, Cs^+ was replaced with Rb^+ in $CsPbBr_3$ via a high-temperature injection method at 120–150 °C. By adjusting the Rb/Cs ratio, blue QD PeLEDs with peak EQEs of 0.87% (490 nm) and 0.11% (464 nm) were prepared. This approach preserves the pure Br crystal structure, avoiding the deep-level defects associated with conventional mixed-anion strategies (Todorović et al., 2019).

According to LaMer theory, QD formation entails three stages—nucleation, growth, and Ostwald ripening (Whitehead et al., 2019). An improved ligand-assisted reprecipitation (LARP) technique utilizing a low precursor concentration, excess lead bromide ($PbBr_2$), and a high ligand concentration significantly slows QD growth and suppresses the Ostwald ripening process. By controlling the precursor temperature under ambient conditions, the size of QDs can be precisely tuned, achieving a wavelength range from 433 to 501 nm, covering the deep-blue region (Fig. 3a). These ultrasmall QDs realized an EQE of 1.0% at 459 nm (Ding et al., 2024).

In addition to the methods mentioned above, a core-shell approach involves purifying the QD solution after achieving blue emission through halide composition adjustment, followed by the introduction of di-n-decyl dimethylammonium chloride (DDAC) to incorporate additional Cl^-. By adjusting the DDAC content, a gradient core-shell structure can be formed in the QDs: a Cl-rich shell with a high Cl concentration on the surface and a Br-rich core with a high Br concentration inside (Figs. 3b and 3c). This structure not only reduces the surface defect density but also enhances the exciton binding energy, achieving a maximum EQE of 4.6% at 465 nm (Xu et al., 2025). In addition, a QD-in-organic solid solution strategy, which disperses $CsPbBr_3$ QDs into N,N′-dicarbazolyl-3,5-benzene (mCP) organic matrix to suppress inter-particle interactions, has been demonstrated to achieve deep-blue emission at 462 nm (y_{CIE}<0.06, where y_{CIE} represents the y-chromaticity coordinate in the CIE color space) with a maximum EQE of 6.2% (Jang et al., 2024).

The Ruddlesden–Popper (RP) phase represents the most prevalent structural form of 2D perovskites, wherein inorganic perovskite octahedral slabs comprising n layers are interleaved with organic or inorganic spacer cations. Accordingly, precise control over the bandgap and emission wavelength in quasi-2D perovskites is achieved by tuning n, which directly governs the extent of quantum confinement. The first one-pot synthesis of nanoscale quasi-2D layered lead bromide perovskites, with the general formula $(RNH_3)_2(MA)_{n-1}Pb_nBr_{3n+1}$, achieved luminescence tuning from deep blue (403 nm) to bright green (530 nm), laying the foundation for subsequent PeLED device fabrication (Yuan et al., 2016). Aromatic polyamines can be used to modulate the low-dimensional components of quasi-2D perovskites. To address the issues of severe non-radiative recombination in the n=1 phase and poor phase stability in deep-blue quasi-2D perovskite devices, the introduction of the aromatic polyamine molecule 1,4-bis(aminomethyl)benzene bromide (P-$PDABr_2$) significantly enhances the stability of quasi-2D perovskites under both high-temperature and high-voltage conditions, achieving a maximum EQE of 2.6% at 465 nm (Yuan et al., 2019).

In traditional quasi-2D perovskites, the top-down crystallization process leads to a vertical gradient

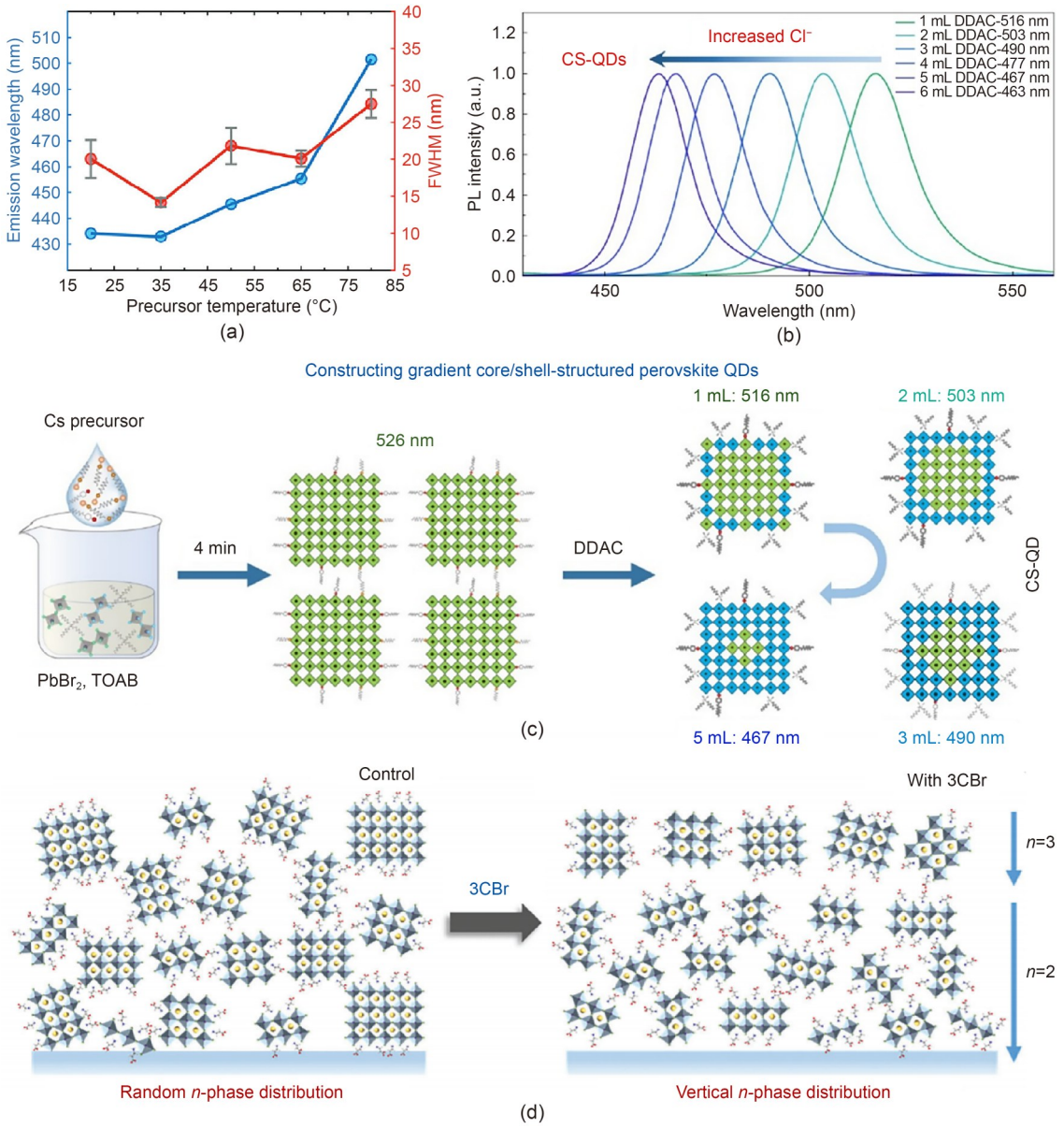

Fig. 3 (a) Variations in the emission wavelength and full width at half maximum (FWHM) of the as-synthesized QDs with precursor temperature (reprinted from (Ding et al., 2024), Copyright 2024, with permission from John Wiley and Sons); (b) PL spectra at 365 nm excitation of core/shell-structured QDs (CS-QDs) with different amounts of DDAC (reprinted from (Xu et al., 2025), Copyright 2025, with permission from American Chemical Society); (c) formation of Cl-rich shells with varying thicknesses by adding different amounts of DDAC (TOAB is the tetra-n-octyl ammonium bromide) (reprinted from (Xu et al., 2025), Copyright 2025, with permission from American Chemical Society); (d) schematic illustration of the spatial *n*-phase distribution for control and 3CBr-treated perovskite films (reprinted from (Dong et al., 2024), Copyright 2024, with permission from John Wiley and Sons)

distribution of *n*-phases: the bottom region consists of small-*n* phases with larger bandgaps and higher activity, while the top region contains large-*n* phases with poorly controlled distribution, which results in multi-peak emission spectra and peak EL wavelength shifts. To address this issue, one approach involves introducing partially ionized amino acid salts such as 3-aminopropanoate bromide (3CBr) to modulate the crystallization kinetics and construct a vertically uniform *n*-phase distribution (Fig. 3d). This method ultimately achieved a peak EQE of 3.64% at 466 nm (Dong et al., 2024). Another approach involves employing a thermal gradient annealing strategy combined with NaBr modulation to construct a vertically concentrated quantum well structure,

achieving a peak EQE of 5.82% at 458 nm (Xia et al., 2024).

2.1.3 Device architecture

In the device structure design of PeLEDs, the core objective of energy level alignment in transport layers is to achieve efficient and balanced charge injection, suppress non-radiative recombination, and consequently enhance the efficiency (Zou et al., 2020). The energy levels of some commonly used transport layer materials are shown in Fig. 4a (Zhang and Long, 2022). Optimizing the energy levels of each layer through ultraviolet photoelectron spectroscopy (UPS) can ensure balanced charge injection. For example, aligning the highest occupied molecular orbital (HOMO) level of the HTL with the valence band maximum (VBM) of the perovskite reduces the injection barrier, thereby lowering the operating voltage and mitigating Joule heating effects (Cho et al., 2018).

Blue perovskite materials typically have a deep VBM around −5.48 eV, making it challenging to find well-matched HTLs, which often leads to unbalanced charge injection and low device efficiency (Yang et al., 2023). Traditional HTLs such as poly(3,4-ethylenedioxythiophene)-poly(styrenesulfonate) (PEDOT:PSS), due to their acidity, can corrode indium tin oxide (ITO) electrodes, releasing indium (In) and tin (Sn) atoms and leading to device degradation. Using a buffered hole injection layer (Buf-HIL), such as a composite of PEDOT:PSS with perfluorinated ionomer (PFI), can suppress electrode corrosion and improve hole injection (Cho et al., 2018). For instance, a structure such as ITO/PEDOT:PSS:PFI/poly[(9,9-dioctylfluorenyl-2,7-diyl)-*alt*-(9-(2-ethylhexyl)-carbazole-3,6-diyl)] (PF8Cz) can create a small hole injection barrier, facilitating hole injection (Fig. 4b) (Gao et al., 2024). CsCl can also cause PEDOT: PSS chains to reorganize from an amorphous state to closely packed grains, promoting charge carrier transport. After modification with CsCl, the work function of PEDOT:PSS can shift from −5.10 to −5.49 eV, providing better alignment with the VBM of perovskite (−5.48 eV), reducing the hole injection barrier, and improving injection efficiency (Fig. 4c) (Chu et al., 2023). Poly(9-vinylcarbazole) (PVK) is another commonly used HTL. Inserting a layer of PFI between the PVK and the perovskite layer can act as an interfacial dipole layer, provide interface passivation, and induce favorable film formation, enabling effective energy level alignment and suppression of non-radiative recombination (Yuan et al., 2019).

Ion migration is a primary cause of the low stability of PeLEDs. Effective suppression through interface engineering can significantly enhance device lifetime. Using small amine molecules or polymers as passivation layers can reduce surface defects and ion migration (Cho et al., 2018). For QDs, core-shell design and ligand engineering are effective methods for improving stability (Cho et al., 2018). Traditional amine ligands tend to accumulate during synthesis, increasing surface defects on perovskite QDs. Z-type ligands, such as zinc oleate, can form strong coordination bonds with bromide ions on the surface of QDs. This helps reduce the accumulation of excess amine ligands and maintains the acid–base balance on the surface (Fig. 4d) (Chen et al., 2024).

2.2 Key challenges

Despite significant progress in recent years, the development of deep-blue devices remains constrained by three interrelated challenges: operational stability, wavelength tunability, and brightness. The wide bandgap, mixed-halide and low-dimensionality of deep-blue perovskites inherently induce deep-level defects, phase segregation, and severe non-radiative recombination, collectively limiting device lifetime, spectral purity, and brightness.

2.2.1 Operational stability

Operational stability remains the primary bottleneck hindering the commercialization of deep-blue PeLEDs. The limited operational stability of deep-blue PeLEDs originates from several factors. (1) The wide bandgap of deep-blue perovskites inherently promotes the formation of deep-level defects, which intensify non-radiative recombination pathways (Liu AQ et al., 2021). (2) Mixed-halide compositions are typically needed for deep-blue emission, which makes these devices vulnerable to ion migration and phase segregation (Ren et al., 2021). (3) Dimensionality control can facilitate deep-blue emission, but low-dimensional perovskite phases exhibit higher carrier concentrations at recombination centers, which promotes Auger recombination and Joule heating, ultimately degrading device performance and stability (Fig. 5a) (Liu XK et al., 2021; Zhao BD et al., 2024).

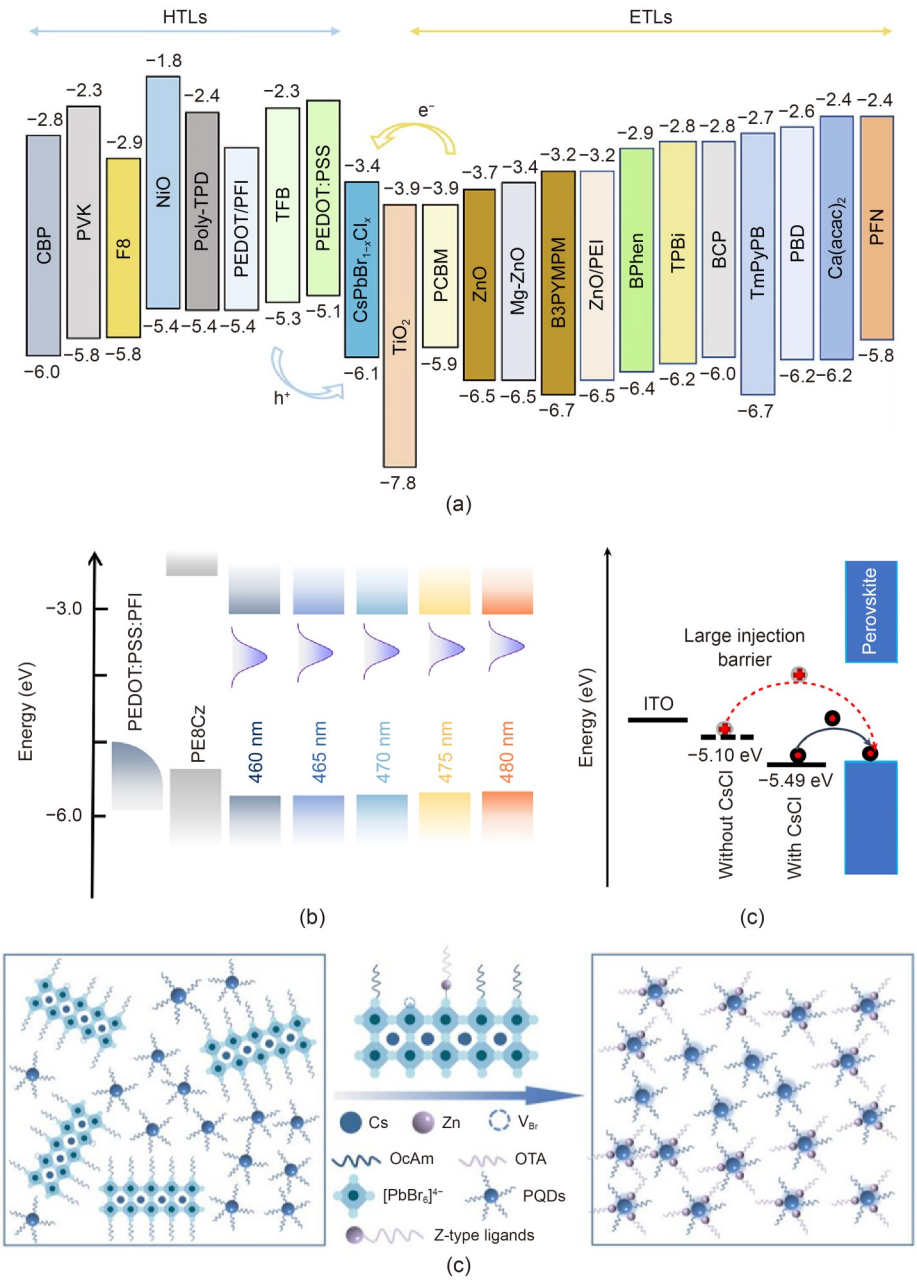

Fig. 4 (a) Energy levels of various functional interlayers with blue emissive perovskites (CBP: 4,4′-bis(9-carbazolyl)-1,1′-biphenyl; F8: poly(9,9-dioctylfluorene); poly-TPD: poly[N,N′-bis(4-butylphenyl)-N,N′-bis(phenyl)benzidine]; TFB: poly[9,9-dioctylfluorene-*co*-N-(4-(3-methylpropyl))diphenylamine]; PCBM: (6,6)-phenyl-C_{61}-butyric acid methyl ester; B3PYMPM: 4,6-bis(3,5-di(pyridine-3-yl)phenyl)-2-methylpyrimidine; PEI: polyethylenimine ethoxylated; BPhen: bathophenanthroline; TPBi: 1,3,5-tris(1-phenyl-1H-benzimidazol-2-yl)benzene; BCP: 2,9-dimethyl-4,7-diphenyl-1,10-phenanthroline; TmPyPB: 1,3,5-tris(3-(pyridine-3-yl)phenyl)benzene; PBD: 2-(4-biphenylyl)-5-phenyl-1,3,4-oxadiazole; $Ca(acac)_2$: calcium bis(acetylacetonate) hydrate; PFN: poly[(9,9-bis(3′-(N,N-dimethylamino)propyl)-2,7-fluorene)-*alt*-2,7-(9,9-dioctylfluorene)]; h^+: hole) (reprinted from (Zhang and Long, 2022), Copyright 2022, with permission from Elsevier); (b) schematic diagram of the energy level, showing PEDOT:PSS:PFI, PF8Cz, and the nanocrystals (reprinted from (Gao et al., 2024), Copyright 2024, with permission from the American Association for the Advancement of Science); (c) band alignment when using PEDOT:PSS with and without CsCl addition as the HIL for PeLEDs (reprinted from (Chu et al., 2023), Copyright 2023, with permission from Springer Nature); (d) schematic illustrating the regulation of the size distribution and acid–base balance in low-dimensional perovskites (V_{Br}: bromine vacancy; OcAm: n-octylamine; OTA: n-octanoic acid; PQDs: perovskite quantum dots) (reprinted from (Chen et al., 2024), Copyright 2024, with permission from American Chemical Society)

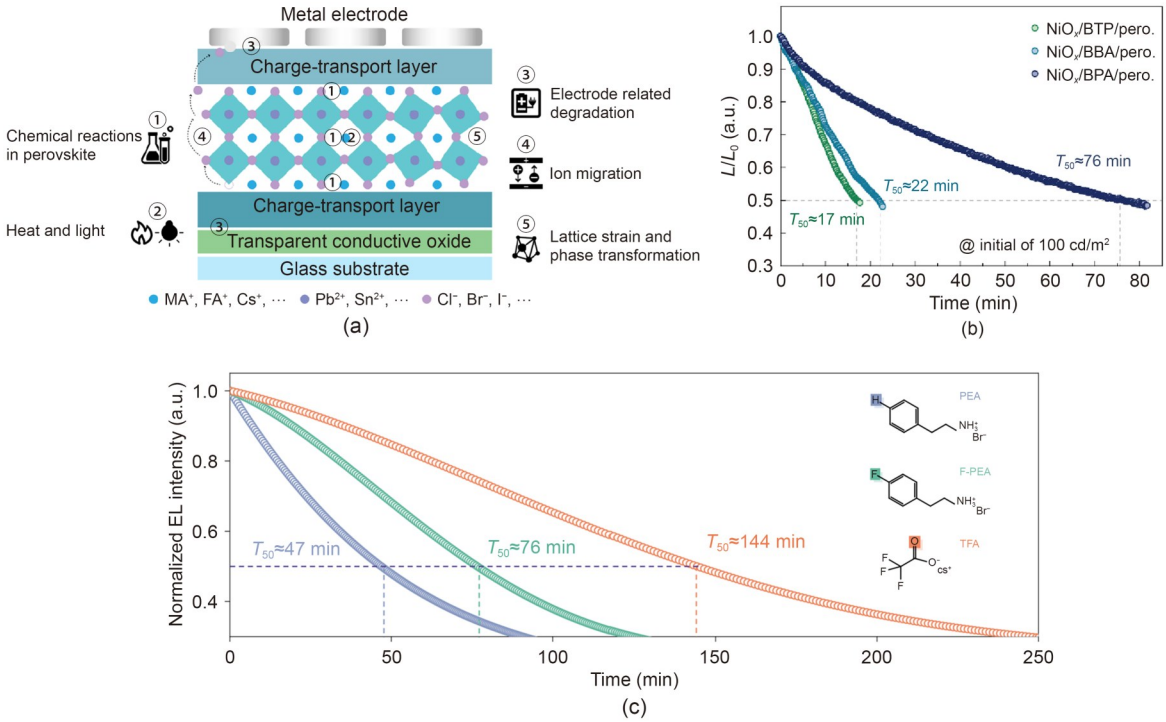

Fig. 5 (a) Key mechanisms of PeLED degradation (reprinted from (Zhao BD et al., 2024), Copyright 2024, with permission from Elsevier); (b) operational stability of NiO_x/BTP-, NiO_x/BBA-, and NiO_x/BPA-based devices under initial luminance of about 100 cd/m^2 in the nitrogen-filled glovebox (BTP: 4-bromophenylthiol; BBA: 4-bromobenzoic acid; BPA: 4-bromophenylphosphonic acid; L: luminance; L_0: initial luminance) (reprinted from (Wei et al., 2026), Copyright 2026, with permission from John Wiley and Sons); (c) half-lifetime measurements at constant current density for three typical PeLEDs (the inset is the molecular structure of phenethylamine (PEA), 4-fluorophenylethylamine (F-PEA), and trifluoroacetate (TFA)) (reprinted from (Dong et al., 2025), Copyright 2025, with permission from Springer Nature)

To mitigate ion migration, enhancing the binding energy of the perovskite lattice is a critical strategy (Liu et al., 2026). A multivalent immobilization strategy was developed by incorporating fluorine- and oxygen-containing small molecules, which leverages a triple synergistic effect to rigidly anchor organic cations and lead-halide octahedra within the lattice. The resulting deep-blue PeLEDs (459 nm) achieved a T_{50} lifetime (the time for the emission intensity to decrease to 50% of the initial value) of 144 min at a high current density of 0.45 mA/cm^2 (Fig. 5c) (Dong et al., 2025). Furthermore, an in-situ chlorination (isCl) strategy was developed, employing p-fluorocinnamoyl chloride (p-FCACl) to release chloride ions while simultaneously transforming into organic ligands, which can reconstruct the quasi-2D phase distribution. Benefiting from this structural optimization and defect passivation, the PeLEDs exhibited excellent spectral stability at 454 nm with an operating lifetime extended to 24.9 min (Yu et al., 2025).

As summarized in Table 1, the state-of-the-art performance of deep-blue PeLEDs currently lags far behind that of their red and green counterparts. It should be noted that direct comparison of T_{50} values across different reports is challenging, as the testing conditions vary considerably, including initial luminance and current density. For deep-blue PeLEDs, few devices have been tested under a consistent initial luminance of 100 cd/m^2, largely because their brightness and stability remain relatively low. Under an initial luminance of 100 cd/m^2, the T_{50} lifetime of deep-blue devices rarely exceeds one hour. A recent study demonstrated a deep-blue PeLED (463 nm) by employing a tridentate anchoring strategy on NiO_x. This approach significantly enhanced interfacial adsorption stability and maintained favorable energy-level alignment during device fabrication. The resulting device achieved a maximum EQE of 15.8% and a T_{50} lifetime of approximately 76 min at an initial luminance of 100 cd/m^2, representing one of the best-performing deep-blue PeLEDs to date (Fig. 5b) (Wei et al., 2026).

However, the current operational lifetime of deep-blue PeLEDs remains far below the standard required

Table 1 Summary of the performance of the recently reported deep-blue PeLEDs

Perovskite	Structural form	Device architecture	EL peak (nm)	CIE coordinates	EQE_{max} (%)	Peak luminance (cd/m^2)	Lifetime	Test condition	Reference
p-FCACl:$PEA_2(Cs_xEA_{1-x}PbBr_yCl_{3-y})_2PbBr_4$	Quasi-2D	ITO/PVK/PVP/perovskite/TPBi/Liq/Al	454	(0.149, 0.025)	6.17	510	T_{50}= 24.9 min	At 0.07 mA/cm^2	Yu et al. (2025)
MS:ES:$CsPbBr_xCl_{3-x}$	3D	ITO/PEDOT:PSS:PFI:FS/perovskite/TPBi/LiF/Al	461	(0.140, 0.039)	5.68	2707	T_{50}= 9.0 min	L_0= 100 cd/m^2	Lee S et al. (2024)
$NaBrPEA_2Cs_{n-1}Pb_n(Cl/Br)_{3n+1}$	Quasi-2D	ITO/PVK/perovskite/TPBi/Liq/Al	458	(0.140, 0.060)	5.82	46.28	T_{50}= 13.4 min	L_0= 19.17 cd/m^2	Xia et al. (2024)
$CsPb(Br/Cl)_3$	Nanocrystal	ITO/PEDOT:PSS/TFB/perovskite/TPBi/LiF/Al	451	(0.170, 0.060)	1.32	2916	T_{50}= 19.8 min	L_0=100 cd/m^2	Hong et al. (2023)
$CsPbBr_3$	QD	ITO/PEDOT:PSS/PTAA/PEABr/perovskite/TPBi/LiF/Al	454	(0.143, 0.040)	4.39	72	T_{50}= 4.5 min	L_0=72 cd/m^2	Chen et al. (2023)
PEABr:$CsPbBr_3$	Quasi-2D	ITO/BPA-modified-NiO_x/perovskite/POT2T/LiF/Al	463	(0.140, 0.060)	15.8	1244	T_{50}= 76 min	L_0=100 cd/m^2	Wei et al. (2026)
F-PEA:TFA:(Cs/PBA/EA/Rb)$PbBr_xCl_{3-x}$	Quasi-2D	ITO/SC-PEDOT/perovskite/TPBi/LiF/Al	459	(0.136, 0.051)	15.4	120	T_{50}= 2.40 h	At 0.45 mA/cm^2	Dong et al. (2025)
PBA:EA:$CsPbBr_xCl_{3-x}$	Quasi-2D	ITO/PEDOT:PSS/perovskite/TPBi/LiF/Al	457	(0.141, 0.053)	4.62	123.3	T_{50}= 1.50 h	L_0=17.2 cd/m^2	Dong et al. (2022)

PBA: phenylbutylamine; PVP: polyvinylpyrrolidone; Liq: 8-hydroxyquinolinato lithium; FS: fluorosurfactant; PTAA: poly[bis(4-phenyl)(2,4,6-trimethylphenyl)amine]; POT2T: 2,4,6-tris[3-(diphenylphosphinyl)phenyl]-1,3,5-triazine; SC: sodium citrate

for commercial applications (>10000 h), necessitating further investigation into the degradation mechanisms of deep-blue PeLEDs and the development of stability optimization strategies.

2.2.2 Wavelength tunability

Adjusting the halide composition offers an effective approach to wavelength tuning in perovskite materials. Partial substitution of Br^- with Cl^- significantly widens the perovskite bandgap, enabling blue emission (Ravi et al., 2016). However, the low solubility of Cl^- leads to degraded film quality, impairing charge transport and radiative recombination efficiency (Akkerman et al., 2015). Moreover, the high migration rate of Cl^- induces phase segregation, resulting in spectral instability and device degradation (Gao et al., 2024). To overcome these challenges, the vapor-assisted crystallization technique (Karlsson et al., 2021) and the in-situ halide exchange method (Tong et al., 2023; Zeng et al., 2023; Zhang et al., 2024; Zhao SH et al., 2024) have been adopted during perovskite film fabrication to suppress ion migration and local heterogeneity.

In addition, wavelength tuning can also be achieved by introducing specific cations to avoid halide mixing. For instance, incorporating A-site ions with relatively small radii, such as Rb^+, induces lattice contraction in

the perovskite, resulting in a blue shift of the emission wavelength (Gao et al., 2024). Meanwhile, substitution of B-site Pb^{2+} with ions such as Sn^{2+}, Cd^{2+}, Mn^{2+}, and Zn^{2+} has been reported for wavelength tuning in deep-blue perovskites (van der Stam et al., 2017). However, such doping typically results in low PLQYs (van der Stam et al., 2017), and excessive doping introduces detrimental strain, leading to unsatisfactory device efficiency and color purity (Ren et al., 2022).

Bandgap tuning for deep-blue emission can also be achieved through reduced-dimensional perovskites (RDPs). A multivalent immobilization strategy incorporating polyfluoro oxygen-containing molecules into RDPs enabled deep-blue (459 nm) PeLEDs with a T_{50} lifetime of 144 min at 0.45 mA/cm^2 (Dong et al., 2025). However, low-dimensional perovskites typically suffer from poor carrier transport capability and severe Auger recombination, which lead to device degradation and adversely affect color purity and brightness (Jiang et al., 2021). Therefore, how to balance the efficiency, brightness, and stability of the device while maintaining deep-blue emission remains a critical topic requiring further investigation.

2.2.3 Brightness

Achieving high luminance in the deep-blue region is more challenging than in the green and red spectral domains. This is primarily due to the deep VBM of deep-blue perovskites, which creates a substantial injection barrier relative to the HTL, and the fact that chloride incorporation typically induces deep-level vacancies, leading to severe non-radiative recombination and efficiency roll-off (Gao et al., 2024). An effective approach involves the targeted passivation of Cl vacancies using sulfonate ligands. The strong coordination between sulfonate groups and Pb^{2+} ions effectively eliminates non-radiative recombination centers, significantly enhancing radiative recombination efficiency. Consequently, deep-blue PeLEDs employing this method demonstrated an exceptional luminance of 2707 cd/m^2 at 461 nm (Lee S et al., 2024). A multifunctional zwitterion, 3-(benzyldimethylammonio) propanesulfonate (3-BAS), has also been introduced to simultaneously passivate surface defects and regulate crystallization kinetics. This approach suppresses low-efficiency small-*n* phases, achieving a high luminance of 1806 cd/m^2 for deep-blue emission (466 nm) (Shen et al., 2024).

Furthermore, the role of light management cannot be overlooked. A bimetallic superlattice top-emission structure was designed for sky-blue PeLEDs (482 nm). By coupling surface plasmons, this architecture significantly enhances light extraction efficiency (LEE), achieving a luminance exceeding 10000 cd/m^2 (Hou et al., 2025). Similarly, incorporating aperiodic funnel-shaped nanoarrays as internal light extraction structures (iLEs) at the HTL/perovskite interface increased the EQE of blue PeLEDs (486 nm) from 12.8% to 16.8% and the maximum luminance from 1390 to 1694 cd/m^2. With the further addition of hemispherical lens as external light extraction structures (eLEs) to extract substrate-mode light, the EQE and luminance reached 27.5% and 3651 cd/m^2, respectively (Shen et al., 2021). Notably, although these optical management strategies have primarily been applied to sky-blue and blue PeLEDs, they hold great promise for deep-blue emitters, where brightness and efficiency are even more severely limited by higher defect densities and poorer charge injection. The design of optical microcavities and light extraction structures may therefore emerge as a key strategy for overcoming the challenge of brightness in deep-blue emitters.

3 Deep-blue lead-free PeLEDs

Metal halide PeLEDs have achieved significant milestones in both efficiency and stability. The EQE of lead-based PeLEDs has already exceeded 30%, with sky-blue PeLEDs (483 nm) reaching 22% (Yuan et al., 2024) and operating lifespans approaching those of OLEDs (Kim et al., 2022). However, the inherent toxicity of lead—specifically its high water solubility and subsequent environmental impact—presents a major barrier to commercialization. Consequently, the development of high-performance lead-free or lead-substituted perovskite materials has emerged as a critical research focus (Ko et al., 2025). Since the initial introduction of methylammonium tin iodide ($MASnI_3$) as a photoactive material, a diverse range of lead-free halide perovskites have been reported (Noel et al., 2014; Tang et al., 2025), encompassing various elemental compositions (Fig. 6a). Nevertheless, the performance of current lead-free PeLEDs remains suboptimal (Fang et al., 2023). This section will detail the material properties of lead-free perovskites, examine the research progress

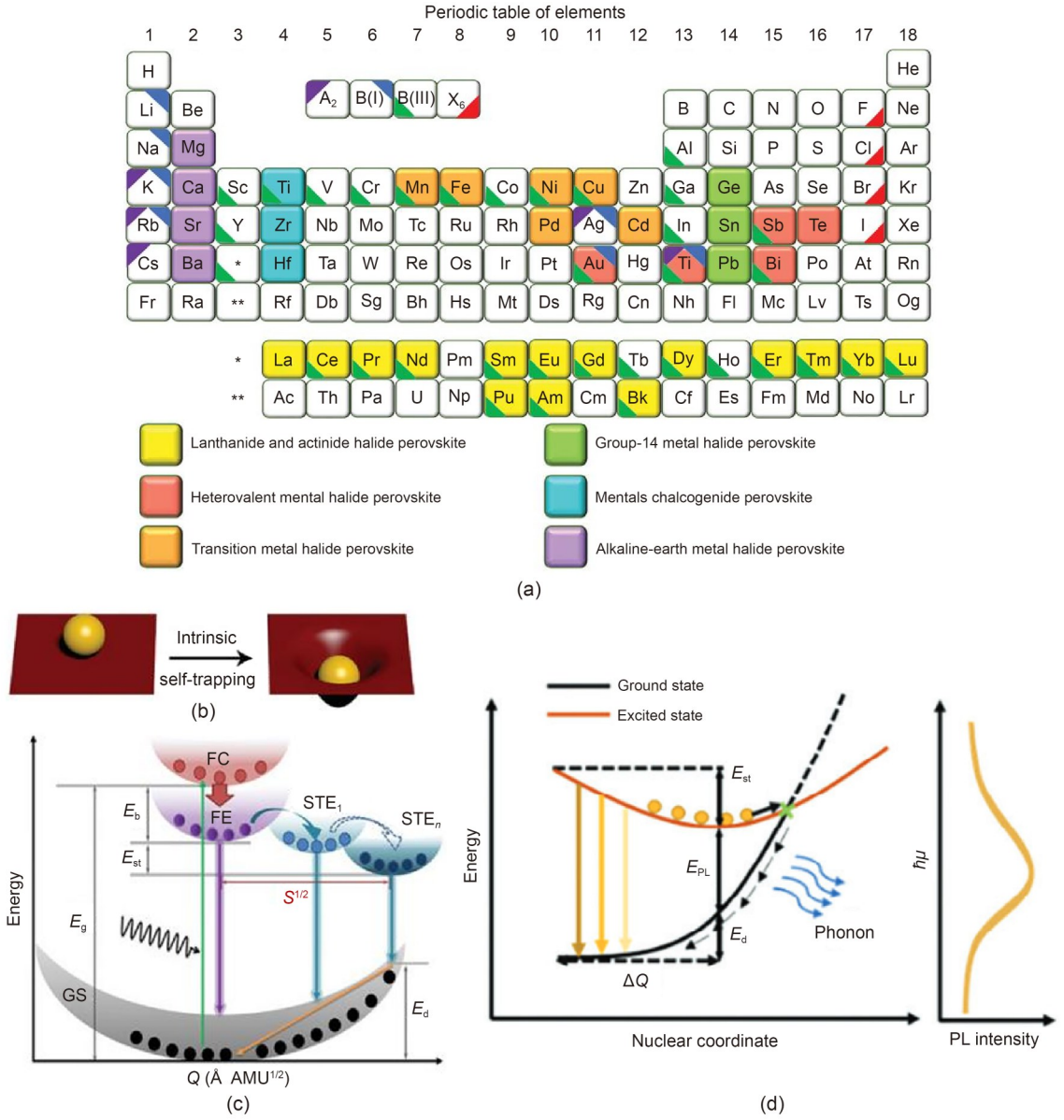

Fig. 6 (a) Candidate elements that may be used as lead substitutes in perovskites (lead replacement candidates in perovskite-type compounds from the periodic table of elements with the focus on homovalent substitution with group-14 elements (Ge, Sn), alkaline-earth metals (Mg, Ca, Sr, Ba), transition metals (Cu, Fe, Pd), lanthanides and actinides (Eu, Tm, Yb), heterovalent substitution with Tl, Au, Sb, Bi, and Te, and metal chalcogenide perovskites (Ti, Zr, Hf)) (Hoefler et al., 2017; Li et al., 2021); (b) schematic illustration showing the self-trapping phenomenon/process (reprinted from (Guo et al., 2022), Copyright 2022, with permission from John Wiley and Sons); (c) configuration coordinate (CC) diagrams illustrating the schematic of the adiabatic potential energy curves of STEs (GS represents the ground state; E_g represents the bandgap; E_b represents the exciton binding energy; E_{st} represents the self-trapping energy; FC represents the free carrier; FE represents the free excitons; S represents the Huang–Rhys factor; E_d represents the lattice distortion energy; Q represents the vibrational coordinate; AMU is the atomic mass unit) (reprinted from (Guo et al., 2022), Copyright 2022, with permission from John Wiley and Sons); (d) diagrams of nonradiative relaxation and broadband emission for STE with large S (E_{PL} represents the emission energy of self-trapped exciton; $\hbar\mu$ represents the energy of phonon, where μ is the angular frequency of phonon) (reprinted from (Zhao JP et al., 2024), Copyright 2024, with permission from John Wiley and Sons)

of deep-blue PeLEDs across different substitution systems, compare their performance against lead-based counterparts, and discuss the primary challenges facing the field.

Lead-free perovskites often exhibit a unique luminescence mechanism, with certain materials relying on the emission of self-trapped excitons (STEs) (Figs. 6b and 6c). A self-trapped state refers to an electronic or hole state localized within a potential well generated by local defects or lattice distortion. These states facilitate the trapping of carriers within low-dimensional structures, rendering low-dimensional materials highly promising for wide-color-gamut optoelectronic applications (Yao et al., 2025). Typical characteristics of STE emission include a broad FWHM, a significant Stokes shift, and a relatively long emission lifetime. This phenomenon, prevalent in materials with soft lattices and strong exciton–phonon coupling, is driven by intense electron-lattice interactions and structural distortions, which can be verified through techniques such as PL spectroscopy (Fig. 6d) (Zhao JP et al., 2024; Chen YM et al., 2025).

However, compared with Pb-based PeLEDs, non-Pb systems without $6s^2$ lone pair electrons show unique defect issues.

3.1 Sn/Zr (II/IV)-based perovskites

Tin-based materials share significant similarities with their lead-based group-IV counterparts, including high carrier mobility and low exciton binding energy (Fang et al., 2023); however, they exhibit anomalously high intrinsic conductivity, owing to their higher activity of $5s^2$ lone pair electrons (Takahashi et al., 2011; Chung et al., 2012). Despite these advantages, several factors continue to impede the performance of tin-based perovskites. Specifically, the rapid crystallization of Sn^{2+} compounds results in poor surface coverage and a high density of pinhole defects. These defects render the material highly susceptible to oxidation (Wong et al., 2018), forming vacancies and inducing self-doping (Gao et al., 2020). In this process, Sn^{2+} is easily oxidized to Sn^{4+}, introducing high concentrations of Sn vacancies as shallow acceptor dopants in the lattice, resulting in unintentional p-type heavy doping and a high carrier concentration, leading to electrical defects. This phenomenon represents a critical bottleneck preventing substantial performance improvements in Sn-based systems. Furthermore, tin-based perovskites typically exhibit strong electron–phonon coupling, which severely quenches blue emission at room temperature (Han et al., 2025), largely because of the stronger covalent nature of the Sn-I bond and softer ionic lattice (Wu et al., 2025). Conversely, Sn^{4+}-based materials have been reported as vacancy-ordered double perovskites with an $A_2B_1B_2X_6$ configuration, demonstrating superior optical stability (Zhao JP et al., 2024).

By synthesizing Cs_2ZrCl_6 nanocrystals, researchers developed a lead-free blue PeLED exhibiting a broad PL peak at 446 nm with a PLQY as high as 60.37% (Liu et al., 2020). Other variants of Sn/Zr-based nanocrystals display a significantly extended broad spectrum spanning 600–1700 nm (Tang et al., 2025).

Among the various categories of lead-free PeLEDs, tin-based systems demonstrate superior performance; however, they suffer from poor ambient stability, necessitating rigorous strategies to prevent the oxidation of Sn^{2+}. These improvements in performance can be realized by enhancing film quality through ligand engineering or utilizing specialized fabrication techniques to completely isolate the material from moisture and oxygen. These methods improve crystalline quality and reduce defect density (Bai et al., 2023), employing effective additives (Zhang et al., 2019; Wang et al., 2021). Additionally, the oxidation of Sn^{2+} can be effectively suppressed, and the perovskite structure can be stabilized through the introduction of additives such as hypophosphorous acid (HPA), Eu^{2+}, and valeric acid (Fang et al., 2023). Furthermore, by introducing rigid organic cation protonated 4-bromobenzylamine ($BrPMA^+$) to significantly reduce electron–phonon coupling, a pure-blue emission at 467 nm was achieved with a maximum EQE of 1.3% and a T_{50} lifetime of 22 min (Han et al., 2025).

3.2 Sb/Bi (III)-based perovskites

The excellent optoelectronic properties of Pb-based perovskites are closely related to the $6s^2$ $6p^0$ electronic configuration of Pb. As less toxic elements, Bi and Sb share the same electronic structure as Pb (Zhao JP et al., 2024). Using ethanol as an anti-solvent, $Cs_3Bi_2Br_9$ QDs can be synthesized, which exhibited a PLQY of 19.4% at 410 nm and showed potential for white light-emitting diodes (WLEDs) (Shen et al., 2020). Despite sharing the same $6s^2$ lone pair electrons, compared to lead-based materials, its +3 valence state leads to a dramatic change in structural dimensions. To maintain electrical neutrality, they form the low-dimensional structure of $A_3B_2X_9$, which results in an extremely poor carrier transport capability due to its intrinsic low electron

dimension. Due to the strong quantum confinement and soft lattice effect of photogenerated carriers, STE is also prone to occur, resulting in broadband emission (Xia et al., 2020).

Compared to tin-based perovskites, Bi-based and Sb-based perovskites possess better stability. However, due to issues such as larger band gaps, a higher density of defects, and poorer carrier transport, the efficiency of PeLEDs based on Bi-based and Sb-based materials remains very low. The PLQY of Bi-based perovskites can be effectively improved by methods such as anti-solvent treatment, doping, and passivation (Zhu et al., 2021).

3.3 Cu (I)-based perovskites

Cu-based perovskites offer the advantages of high PLQY, good stability, and non-toxicity. Furthermore, their unique emission mechanism contributes to better performance (Fang et al., 2023). Cu^{+}-based perovskites have a full-subshell electronic configuration of d^{10}, which gives their valence band (composed of Cu d orbitals and X p orbitals hybridized) strong Cu d orbital characteristics. Carriers are confined in isolated $[Cu_xX_y]$ polyhedra, rendering interband transport difficult and leading to low carrier mobility. In the 0D crystal structure typically formed by this material, strong exciton–phonon coupling causes local lattice distortion in the excited state, forming STE. Comprehensively, the confined structure and STE make electrons and holes much easier to combine but harder to migrate towards the luminescent center under charge injection. This explains its high PLQY, large Stokes shift, wide spectral emission, and relatively low EQE (Ji et al., 2026).

Although Cu-based perovskites suffer from issues of excessively low efficiency caused by poor charge transport and wide optical band gaps, these can be ameliorated by improving the device structure and film morphology, as well as introducing additives (Chen et al., 2021a).

A low-temperature inorganic solution process was employed to synthesize $Cs_3Cu_2Br_5$ powder, which exhibited blue light emission at 458 nm with a high PLQY of 92%. The same research also described strong green and yellow light emissions from a double perovskite structure, which was achieved by substituting the element at the C-site. This modified material was subsequently used to fabricate a WLED device with a remarkable color rendering index (CRI) of 98, thus demonstrating significant application potential (Chen YM et al., 2025).

High-quality $CsCu_2Br_3$ single crystals were synthesized via an optimized anti-solvent crystallization method, resulting in emission at 451.6 nm with an FWHM of 250.2 nm (Bouzidi et al., 2025).

0D $Cs_3Cu_2I_5$ crystals have been synthesized using the room-temperature solvent evaporation crystallization method. These crystals showed intense blue emission at 442 nm with a PLQY as high as 89%, which is promising for the preparation of fluorescent inks and displays (Zhang et al., 2020). Furthermore, similar 0D $Cs_3Cu_2I_5$ nanocrystals were prepared by a modified hot-injection method, and a PeLED with 445 nm emission, color coordinates of (0.16, 0.07), an EQE approaching 1.10%, and a lifetime up to 108 h was demonstrated (Wang et al., 2020).

3.4 Double perovskites

Lead-free double perovskites refer to materials with a 3D $A_2B^{+}B^{3+}X_6$ framework (Guo et al., 2022). By substituting one B-site cation with a tetravalent ion and creating a vacancy at the other site, vacancy-ordered cubic double perovskites (A_2BX_6) can be formed. The A/B/X-sites offer multiple choices, forming a rich material library that potentially provides solutions for enhancing stability and optoelectronic performance (Tang et al., 2025). Bi-doped Cs_2SnCl_6 double perovskites were synthesized, which emit deep-blue light at 455 nm with a PLQY of 78.9% (Figs. 7a and 7b). The high PLQY is attributed to the Bi ions acting as luminescent centers and partially substituting the tin sites (Tan et al., 2018).

3.5 Other lead-free materials

Rare earth elements (REEs) used as lead-free substitutes are gaining increasing research attention (Tang et al., 2025), mainly due to their unique emission. For example, the primary emission mechanisms of lanthanide halide compounds involve 5d→4f and 4f→4f transitions, which possess higher probability and efficiency (Luo et al., 2021; Yao et al., 2025) (Figs. 7c and 7d). This emission mechanism is less affected by the crystal field and is essentially an atomic spectral feature. This is fundamentally different from the band edge or defect state luminescence of perovskite excitons. Specifically, for the Eu^{2+} system, the luminescence efficiency in wide bandgap matrices is highly dependent

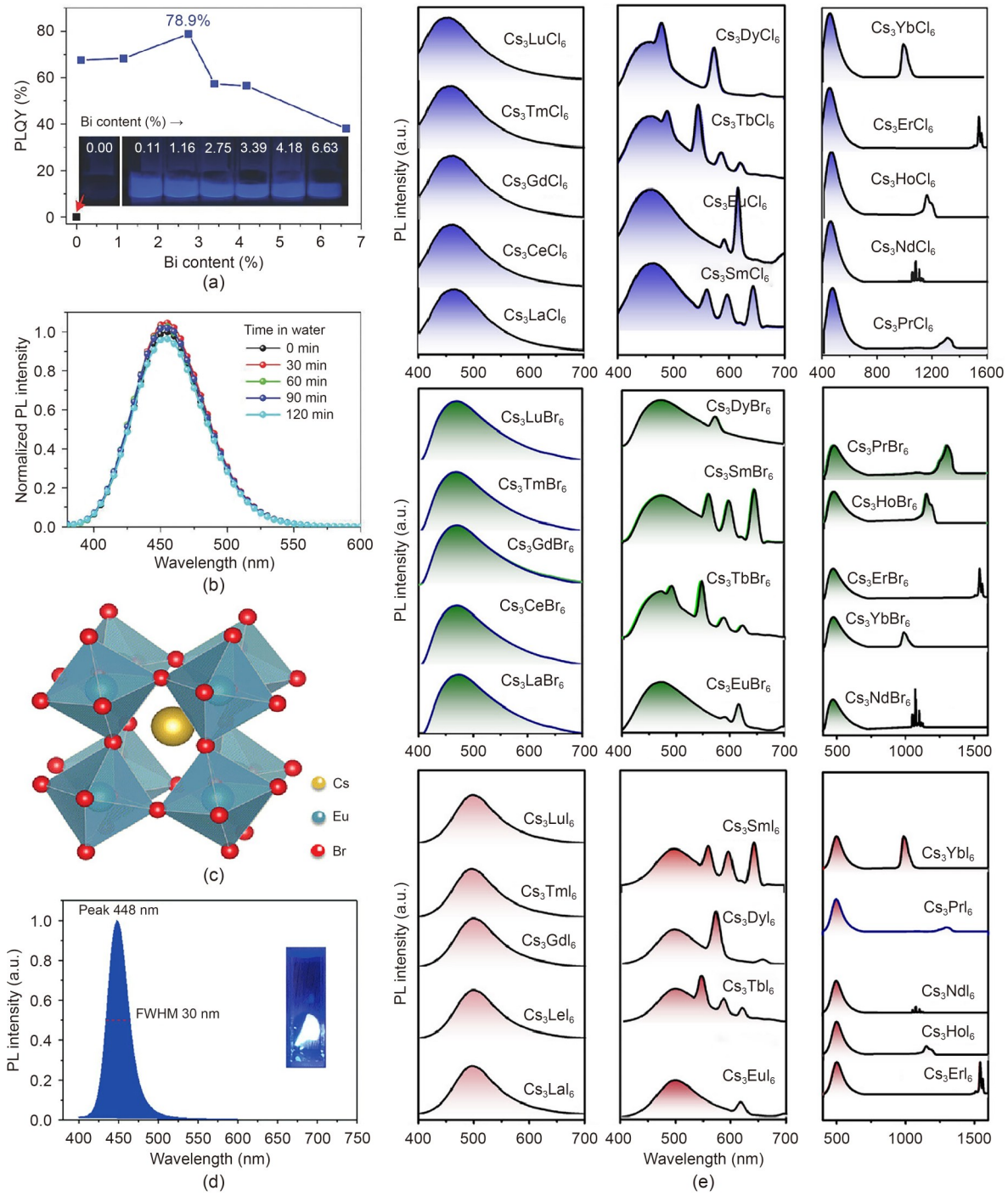

Fig. 7 (a) Room temperature PLQY of Cs_2SnCl_6:*x*Bi with variable *x* (the inset shows photos of Cs_2SnCl_6:*x*Bi under 365 nm ultraviolet (UV) light illumination; the white values in the inset indicate the *x* values) (reprinted from (Tan et al., 2018), Copyright 2018, with permission from John Wiley and Sons); (b) anti-water stability of Cs_2SnCl_6:2.75%Bi immersed in deionized water for different durations (reprinted from (Tan et al., 2018), Copyright 2018, with permission from John Wiley and Sons); (c) basic properties of the lead-free $CsEuBr_3$ structure diagram (reprinted from (Luo et al., 2021), Copyright 2021, with permission from John Wiley and Sons); (d) PL spectrum of $CsEuBr_3$ crystals with 365 nm UV excitation at room temperature (the inset shows the photograph of $CsEuBr_3$ under 365 nm UV light) (reprinted from (Luo et al., 2021), Copyright 2021, with permission from John Wiley and Sons); (e) emission spectra of a series of Cs_3BX_6 structures, where B is REE and X is Cl, Br, or I (reprinted from (Wang et al., 2025), Copyright 2025, with permission from John Wiley and Sons)

on the defect chemical environment generated by its substitution, which determines how excess positive charges are compensated and how Eu^{2+} disperses in the lattice (Li X et al., 2024).

The synthesis of 12 highly luminescent and environmentally friendly deep-blue emitting Eu^{2+}-doped alkali metal halides was reported. By tuning the coordination environment, highly efficient deep-blue Eu-5d→4f transitions were achieved. Among these, $CsBr:Eu^{2+}$ nanocrystals exhibited a high PLQY of 91.1% at 441 nm. The color coordinates at (0.158, 0.023) matched the Rec. 2020, and the EQE reached 3.15%, with a T_{50} approaching 1 h (Li X et al., 2024).

Forty-two types of lanthanide coordination perovskite materials (LCPMs) have been reported, whose nanocrystals, Cs_3LnX_6 (Ln=La, Ce, ⋯, Lu; X=Cl, Br, and I), exhibited an adjustable direct bandgap of 3.1–3.7 eV and achieved an EQE of 5.5% for blue emission at 478 nm (Fig. 7e). Based on ultrafast dynamics and theoretical calculations, they proposed a mechanism involving STE emission and the Förster resonance energy transfer (FRET) process between excitons and lanthanide ions (Wang et al., 2025).

4 Summary and outlook

PeLEDs show great potential in displays and lighting due to their unique advantages, including high color purity, high efficiency, high brightness, and tunable wavelength (Tan et al., 2014). Despite remarkable advances in red and green PeLEDs, the performance of blue PeLEDs, especially in the deep-blue region, remains a critical bottleneck (Ko et al., 2025). We discussed strategies employed to enhance the performance of deep-blue PeLEDs, including compositional engineering, dimensionality control, and device architecture optimization. Focusing on deep-blue PeLEDs, precise control of the bandgap is necessary. Employing Br-Cl mixing is a common approach (Protesescu et al., 2015). To address the increased defect density and performance degradation caused by mixed halides, strategies such as vapor-assisted crystallization (Karlsson et al., 2021) and in-situ halide exchange (Tong et al., 2023; Zeng et al., 2023) have been developed. Substitution at the A-site with Rb^+ or K^+ (Gao et al., 2024; Cao et al., 2025) or at the B-site with Zn^{2+}, Cd^{2+}, or Sr^{2+} (van der Stam et al., 2017; Chen Y et al., 2025) has also been demonstrated to regulate the bandgap. Additionally, low-dimensional perovskites can achieve an increased bandgap through quantum confinement effects without relying on mixed halides (Ding et al., 2024).

Despite the numerous strategies proposed, research on deep-blue PeLEDs still faces significant challenges. The ion migration and halide segregation associated with mixed halides, combined with the poor carrier transport capability and severe Auger recombination in low-dimensional perovskites, result in unsatisfactory operational lifetime and luminance for deep-blue PeLEDs, falling far short of the standards required for commercial applications. Further investigation into the crystallization, non-radiative losses, and aging mechanisms is essential to realize efficient, bright, and stable deep-blue emitters. Optical management and light extraction engineering may emerge as critical breakthrough directions (Zhao et al., 2023).

In addition, achieving lead-free composition represents a crucial pathway for PeLED development. There is currently a scarcity of lead-free perovskite emitters that can achieve deep-blue emission, and the performance of lead-free blue PeLEDs remains relatively poor, characterized by low EQE under electrical injection and unsatisfactory PLQY under photoexcitation (Table 2). According to the literature providing explicit performance metrics, these lead-free deep-blue devices exhibit limited operational lifetimes and low luminance, remaining far from commercial viability. Ongoing research is needed for new material designs and lead-free device optimization, paving the way for PeLEDs to evolve into a genuinely eco-friendly technology.

From a commercialization perspective, several additional bottlenecks must be addressed. First, the operational lifetime of deep-blue PeLEDs (typically T_{50}<1 h at 100 cd/m^2) remains orders of magnitude below the thousands to tens of thousands of hours required for display applications. Second, spectral stability under electrical bias, particularly in mixed-halide systems, remains a critical concern. Third, scalable fabrication methods compatible with industrial production need further development, as most high-performance devices to date have been fabricated by spin-coating, which suffers from poor reproducibility. In terms of fabrication processes, vacuum thermal evaporation has attracted significant attention, as it enables high-resolution, multicolor pattern deposition on various substrates, meeting

Table 2 Summary of the emission performances of lead-free deep-blue perovskite materials and PeLEDs. The empty parts in the table indicate that the items were not presented in the original papers

System	Structural form	Device architecture	PL peak (nm)	CIE coordinates	EQE (%)	PLQY (%)	Peak luminance (cd/m^2)	Lifetime	Test conditions	Reference
$Cs_3Cu_2I_5$	0D (thin film)	ITO/ZSO/perovskite/NPD/MoO_x/Ag	445	(0.150, 0.090)		60.0	10			Jun et al. (2018)
$Cs_3Cu_2I_5$	0D (single crystal)		445	(0.150, 0.090)		90.0				Jun et al. (2018)
Cs_2SnCl_6: Bi	0D		455			78.9				Tan et al. (2018)
$Cs_3Cu_2I_5$	0D	Crystals on PVDF	442	(0.154, 0.118)		89.0				Zhang et al. (2020)
Cs_2ZrCl_6	Nanocrystal		446			60.4				Liu et al. (2020)
$Cs_3Cu_2Br_5$	0D		458			92.0				Chen Y et al. (2025)
$CsEuBr_3$	Bulk	ITO/LiF/perovskite/LiF/TPBi/LiF/Al	448	(0.157, 0.048)	6.50	68.3	58.5	T_{50}= 50 min	L_0= 15.9 cd/m^2	Luo et al. (2021)
$Cs_3Cu_2I_5$	Nanocrystal	ITO/NiO_x/perovskite/TPBi/LiF/Al	445	(0.160, 0.070)	1.10	87.0	263.2	T_{50}= 108 h	L_0= 100 cd/m^2	Wang et al. (2020)
Cs_3LaCl_6	Nanocrystal	ITO/PEDOT:PSS/PVK/perovskite/TPBi/LiF/Al	442		0.53	92.0	127			Sun et al. (2024)
$CsBr:Eu^{2+}$	Nanocrystal	ITO/PEDOT:PSS/TFB/perovskite/TPBi/LiF/Al	441	(0.158, 0.023)	3.15	91.1	311.8	T_{50}=1 h	L_0= 100 cd/m^2	Li X et al. (2024)
$FA_3Bi_2Br_9$	QD	$FA_3Bi_2Br_9$ QDs/PS composites with UV light chips	437	(0.163, 0.130)	3.05	52.0				Shen et al. (2020)

ZSO: zinc silicate; NPD: N,N′-bis-(1-naphthalenyl)-N,N′-bis-phenyl-(1,1′-biphenyl)-4,4′-diamine; PVDF: polyvinylidene fluoride; PS: polystyrene

the manufacturing demands of AR/VR displays (Lee GH et al., 2024). New techniques such as vapor-assisted crystallization can reduce halide segregation and ion migration, enhancing both spectral stability and device efficiency (Karlsson et al., 2021). Compatibility with emerging display technologies, including micro-LEDs and AR/VR systems, also requires consideration; vapor-assisted crystallization and other solvent-free methods may be particularly suitable for uniform film deposition over patterned substrates in micro-display pixel arrays.

In brief, research on deep-blue PeLEDs remains highly significant, and extensive further investigation is necessary. It helps explore the limits of wide-bandgap perovskite luminescence and can spur the development of superior micro/nano fabrication techniques. Beyond displays, deep-blue PeLEDs also hold substantial application potential in lighting, lithography, and other fields.

Acknowledgments

This work is supported by the National Natural Science Foundation of China (Nos. 62274144 and 62405279), the Scientific Research Innovation Capability Support Project for Young Faculty (No. ZYGXQNJSKYCXNLZCXM-I25), the

Fundamental Research Funds for the Central Universities (No. 226-2025-00188), the Zhejiang Provincial Government, and the Haining Municipal Government, China.

Author contributions

Zhuoyue GU and Zhengyang JU drafted the outline of the review paper under the guidance of Baodan ZHAO; Zhuoyue GU, Zhengyang JU, Kecong REN, Feiyang ZHANG, and Shuailiang SHEN wrote the initial draft of the manuscript, which was revised by Baodan ZHAO and Dawei DI.

Conflict of interest

Zhuoyue GU, Zhengyang JU, Kecong REN, Feiyang ZHANG, Shuailiang SHEN, Dawei DI, and Baodan ZHAO declare that they have no conflict of interest.

Declaration on the use of generative AI tools

During the preparation of this work, the authors used DeepSeek to improve language and readability. After using this tool, the authors reviewed and edited the content as needed and take full responsibility for the content of the publication.

Data availability

The data that support the findings of this study are available from the corresponding author upon reasonable request.

References

Akkerman QA, D'Innocenzo V, Accornero S, et al., 2015. Tuning the optical properties of cesium lead halide perovskite nanocrystals by anion exchange reactions. *Journal of the American Chemical Society*, 137(32):10276-10281. https://doi.org/10.1021/jacs.5b05602

Bai WH, Liang MM, Xuan TT, et al., 2023. Ligand engineering enables efficient pure red tin-based perovskite light-emitting diodes. *Angewandte Chemie*, 135(50):e202312728. https://doi.org/10.1002/ange.202312728

Bouzidi M, Alatawi AA, Alkathiri T, et al., 2025. Stable blue emission and sub-gap mediated UV photodetection in lead-free 1D $CsCu_2Br_3$ single crystals. *Scientific Reports*, 15:35882. https://doi.org/10.1038/s41598-025-19735-8

Butkus J, Vashishtha P, Chen K, et al., 2017. The evolution of quantum confinement in $CsPbBr_3$ perovskite nanocrystals. *Chemistry of Materials*, 29(8):3644-3652. https://doi.org/10.1021/acs.chemmater.7b00478

Cao YB, Fu Y, Zhou Y, et al., 2025. Ultrapure and efficient electroluminescence in alkali metal doped inorganic perovskite quantum wires arrays. *Nature Communications*, 16(1):6053. https://doi.org/10.1038/s41467-025-61085-6

Chen H, Zhu L, Xue C, et al., 2021a. Efficient and bright warm-white electroluminescence from lead-free metal halides. *Nature Communications*, 12(1):1421. https://doi.org/10.1038/s41467-021-21638-x

Chen H, Li MH, Wang B, et al., 2021b. Structure, electronic and optical properties of $CsPbX_3$ halide perovskite: a first-principles study. *Journal of Alloys and Compounds*, 862:158442. https://doi.org/10.1016/j.jallcom.2020.158442

Chen Y, Wang RS, Kusch G, et al., 2025. All-site alloyed perovskite for efficient and bright blue light-emitting diodes. *Nature Communications*, 16(1):3254. https://doi.org/10.1038/s41467-025-58470-6

Chen YF, Lu S, Nan M, et al., 2023. Deep-blue $CsPbBr_3$ perovskite quantum dots via green polar solvent and short ligand engineering towards highly efficient light-emitting diodes. *Advanced Optical Materials*, 11(18):2300473. https://doi.org/10.1002/adom.202300473

Chen YF, Nan M, He YX, et al., 2024. Z-type ligand enables efficient and stable deep-blue perovskite light-emitting diodes. *ACS Applied Materials & Interfaces*, 16(17):22139-22146. https://doi.org/10.1021/acsami.4c01824

Chen YM, Zhu HY, Babaian D, et al., 2025. Near-unity PLQY of $Cs_3Cu_2X_5$ (X=Cl, Br) for high-efficiency white light-emitting diodes with exceptional color quality. *Advanced Materials*, 37(21):2500083. https://doi.org/10.1002/adma.202500083

Cheng L, Yi C, Tong YF, et al., 2020. Halide homogenization for high-performance blue perovskite electroluminescence. *Research*, 2020:9017871. https://doi.org/10.34133/2020/9017871

Cho H, Kim YH, Wolf C, et al., 2018. Improving the stability of metal halide perovskite materials and light-emitting diodes. *Advanced Materials*, 30(42):1704587. https://doi.org/10.1002/adma.201704587

Chu ZM, Zhang W, Jiang J, et al., 2023. Blue light-emitting diodes based on quasi-two-dimensional perovskite with efficient charge injection and optimized phase distribution via an alkali metal salt. *Nature Electronics*, 6(5):360-369. https://doi.org/10.1038/s41928-023-00955-7

Chung I, Song JH, Im J, et al., 2012. $CsSnI_3$: semiconductor or metal? High electrical conductivity and strong near-infrared photoluminescence from a single material. High hole mobility and phase-transitions. *Journal of the American Chemical Society*, 134(20):8579-8587. https://doi.org/10.1021/ja301539s

Ding PB, Ko PK, Geng P, et al., 2024. Strongly confined and spectrally tunable $CsPbBr_3$ quantum dots for deep blue QD-LEDs. *Advanced Optical Materials*, 12(11):2302477. https://doi.org/10.1002/adom.202302477

Dong F, Guo YY, Zhang X, et al., 2024. Partially ionized amino acid salt enabling spatially vertical *n*-phase distribution of quasi-2D perovskite for efficient deep-blue light-emitting diodes. *Advanced Optical Materials*, 12(28):2401247. https://doi.org/10.1002/adom.202401247

Dong JC, Lu FF, Han DY, et al., 2022. Deep-blue electroluminescence of perovskites with reduced dimensionality achieved by manipulating adsorption-energy differences. *Angewandte Chemie International Edition*, 61(40):e202210322. https://doi.org/10.1002/anie.202210322

Dong JC, Zhao B, Ji HY, et al., 2025. Multivalent-effect immobilization of reduced-dimensional perovskites for efficient and spectrally stable deep-blue light-emitting diodes.

Nature Nanotechnology, 20(4):507-514. https://doi.org/10.1038/s41565-024-01852-6

Fang WH, Zhang LJ, Lu GH, et al., 2023. Preparation and research progress of lead-free perovskite light emitting diodes. *Chinese Journal of Luminescence*, 44(8):1422-1438. https://doi.org/10.37188/CJL.20230017

Feng SC, Shen Y, Hu XM, et al., 2024. Efficient and stable red perovskite light-emitting diodes via thermodynamic crystallization control. *Advanced Materials*, 36(44):2410255. https://doi.org/10.1002/adma.202410255

Gao CC, Jiang YZ, Sun CJ, et al., 2020. Multifunctional naphthol sulfonic salt incorporated in lead-free 2D tin halide perovskite for red light-emitting diodes. *ACS Photonics*, 7(8):1915-1922. https://doi.org/10.1021/acsphotonics.0c00497

Gao Y, Cai QT, He YF, et al., 2024. Highly efficient blue light-emitting diodes based on mixed-halide perovskites with reduced chlorine defects. *Science Advances*, 10(29): eado5645. https://doi.org/10.1126/sciadv.ado5645

Guo QX, Zhao X, Song BX, et al., 2022. Light emission of self-trapped excitons in inorganic metal halides for optoelectronic applications. *Advanced Materials*, 34(52):2201008. https://doi.org/10.1002/adma.202201008

Han TH, Jang KY, Dong YT, et al., 2022. A roadmap for the commercialization of perovskite light emitters. *Nature Reviews Materials*, 7(10):757-777. https://doi.org/10.1038/s41578-022-00459-4

Han Y, Guo ZY, Liu SC, et al., 2025. Manipulating electron-phonon coupling for efficient tin halide perovskite blue LEDs. *Advanced Materials*, 37(25):2413895. https://doi.org/10.1002/adma.202413895

Hoefler SF, Trimmel G, Rath T, 2017. Progress on lead-free metal halide perovskites for photovoltaic applications: a review. *Monatshefte für Chemie–Chemical Monthly*, 148(5): 795-826. https://doi.org/10.1007/s00706-017-1933-9

Hong YJ, Yu CNM, Je H, et al., 2023. Perovskite nanocrystals protected by hermetically sealing for highly bright and stable deep-blue light-emitting diodes. *Advanced Science*, 10(23):2302906. https://doi.org/10.1002/advs.202302906

Hou HY, Ge HR, Zeng XY, et al., 2025. Bimetallic superlattice enhances efficiency and stability of top-emitting perovskite light-emitting diodes. *ACS Applied Materials & Interfaces*, 17(23):34171-34181. https://doi.org/10.1021/acsami.5c03812

Jang KY, Hwang SY, Woo SJ, et al., 2024. Efficient deep-blue light-emitting diodes through decoupling of colloidal perovskite quantum dots. *Advanced Materials*, 36(39):2404856. https://doi.org/10.1002/adma.202404856

Ji YQ, Wang YQ, Yuan ZX, et al., 2026. Structural modulation enables bright and efficient Cs–Cu–Cl electroluminescence. *Advanced Materials*, 38(15):e22256. https://doi.org/10.1002/adma.202522256

Jiang MW, Li L, Qi ZW, et al., 2025. Efficient Rec. 2020 compliant pure-green mixed-cation perovskite light-emitting diodes with multifunctional co-additives. *Advanced Materials*, 37(29):2503683. https://doi.org/10.1002/adma.202503683

Jiang YZ, Cui MH, Li SS, et al., 2021. Reducing the impact of Auger recombination in quasi-2D perovskite light-emitting diodes. *Nature Communications*, 12(1):336. https://doi.org/10.1038/s41467-020-20555-9

Jun T, Sim K, Iimura S, et al., 2018. Lead-free highly efficient blue-emitting $Cs_3Cu_2I_5$ with 0D electronic structure. *Advanced Materials*, 30(43):1804547. https://doi.org/10.1002/adma.201804547

Karlsson M, Yi ZY, Reichert S, et al., 2021. Mixed halide perovskites for spectrally stable and high-efficiency blue light-emitting diodes. *Nature Communications*, 12(1):361. https://doi.org/10.1038/s41467-020-20582-6

Kim JS, Heo JM, Park GS, et al., 2022. Ultra-bright, efficient and stable perovskite light-emitting diodes. *Nature*, 611(7937): 688-694. https://doi.org/10.1038/s41586-022-05304-w

Ko PK, Ge JC, Ding PB, et al., 2025. The deepest blue: major advances and challenges in deep blue emitting quasi-2D and nanocrystalline perovskite LEDs. *Advanced Materials*, 37(23):2407764. https://doi.org/10.1002/adma.202407764

Lee GH, Kim K, Kim Y, et al., 2024. Recent advances in patterning strategies for full-color perovskite light-emitting diodes. *Nano-Micro Letters*, 16(1):45. https://doi.org/10.1007/s40820-023-01254-8

Lee S, Kim J, Kim H, et al., 2024. Brightening deep-blue perovskite light-emitting diodes: a path to Rec. 2020. *Science Advances*, 10(20):eadn8465. https://doi.org/10.1126/sciadv.adn8465

Li MM, Yang YG, Kuang ZY, et al., 2024. Acceleration of radiative recombination for efficient perovskite LEDs. *Nature*, 630(8017):631-635. https://doi.org/10.1038/s41586-024-07460-7

Li N, Xia Y, He XY, et al., 2026. Dual-B-site strategy underpins stable unimodal deep-blue emitting perovskites. *Advanced Materials*, 38(7):e17517. https://doi.org/10.1002/adma.202517517

Li X, Gao XP, Zhang XT, et al., 2021. Lead-free halide perovskites for light emission: recent advances and perspectives. *Advanced Science*, 8(4):2003334. https://doi.org/10.1002/advs.202003334

Li X, Chen X, Jiang HF, et al., 2024. Efficient deep-blue light-emitting diodes from highly luminescent Eu^{2+}-doped alkali metal halide nanocrystals via lattice field modulation. *Nano Letters*, 24(22):6601-6609. https://doi.org/10.1021/acs.nanolett.4c01155

Liu AQ, Bi CH, Guo RQ, et al., 2021. Electroluminescence principle and performance improvement of metal halide perovskite light-emitting diodes. *Advanced Optical Materials*, 9(18):2002167. https://doi.org/10.1002/adom.202002167

Liu SP, Yang B, Chen JS, et al., 2020. Efficient thermally activated delayed fluorescence from all-inorganic cesium zirconium halide perovskite nanocrystals. *Angewandte Chemie International Edition*, 59(49):21925-21929. https://doi.org/10.1002/anie.202009101

Liu WW, Qiao YK, Deng YY, et al., 2026. Advancements and challenges of highly efficient and stable perovskite light-emitting diodes. *Laser & Photonics Reviews*, 20(2):e01787. https://doi.org/10.1002/lpor.202501787

Liu XK, Xu WD, Bai S, et al., 2021. Metal halide perovskites for light-emitting diodes. *Nature Materials*, 20(1):10-21. https://doi.org/10.1038/s41563-020-0784-7

Luo JJ, Yang LB, Tan ZF, et al., 2021. Efficient blue light emitting diodes based on europium halide perovskites. *Advanced Materials*, 33(38):2101903. https://doi.org/10.1002/adma.202101903

Noel NK, Stranks SD, Abate A, et al., 2014. Lead-free organic–inorganic tin halide perovskites for photovoltaic applications. *Energy & Environmental Science*, 7(9):3061-3068. https://doi.org/10.1039/C4EE01076K

Protesescu L, Yakunin S, Bodnarchuk MI, et al., 2015. Nanocrystals of cesium lead halide perovskites ($CsPbX_3$, X=Cl, Br, and I): novel optoelectronic materials showing bright emission with wide color gamut. *Nano Letters*, 15(6):3692-3696. https://doi.org/10.1021/nl5048779

Ravi VK, Markad GB, Nag A, 2016. Band edge energies and excitonic transition probabilities of colloidal $CsPbX_3$ (X=Cl, Br, I) perovskite nanocrystals. *ACS Energy Letters*, 1(4):665-671. https://doi.org/10.1021/acsenergylett.6b00337

Ren ZW, Wang K, Sun XW, et al., 2021. Strategies toward efficient blue perovskite light-emitting diodes. *Advanced Functional Materials*, 31(30):2100516. https://doi.org/10.1002/adfm.202100516

Ren ZW, Sun JY, Yu JH, et al., 2022. High-performance blue quasi-2D perovskite light-emitting diodes via balanced carrier confinement and transfer. *Nano-Micro Letters*, 14(1):66. https://doi.org/10.1007/s40820-022-00807-7

Shan QS, Dong YH, Xiang HY, et al., 2024. Perovskite quantum dots for the next-generation displays: progress and prospect. *Advanced Functional Materials*, 34(36):2401284. https://doi.org/10.1002/adfm.202401284

Shen C, Fang SY, Zhang JB, et al., 2024. High performance and stable pure-blue quasi-2D perovskite light-emitting diodes by multifunctional zwitterionic passivation engineering. *Advanced Photonics*, 6(2):026002. https://doi.org/10.1117/1.AP.6.2.026002

Shen Y, Wu HY, Li YQ, et al., 2021. Interfacial nucleation seeding for electroluminescent manipulation in blue perovskite light-emitting diodes. *Advanced Functional Materials*, 31(45):2103870. https://doi.org/10.1002/adfm.202103870

Shen YL, Yin J, Cai B, et al., 2020. Lead-free, stable, high-efficiency (52%) blue luminescent $FA_3Bi_2Br_9$ perovskite quantum dots. *Nanoscale Horizons*, 5(3):580-585. https://doi.org/10.1039/C9NH00685K

Sun LH, Dong B, Sun J, et al., 2024. Efficient and stable multicolor emissions of the Coumarin-Modified Cs_3LnCl_6 lead-free perovskite nanocrystals and LED application. *Advanced Materials*, 36(18):2310065. https://doi.org/10.1002/adma.202310065

Takahashi Y, Obara R, Lin ZZ, et al., 2011. Charge-transport in tin-iodide perovskite $CH_3NH_3SnI_3$: origin of high conductivity. *Dalton Transactions*, 40(20):5563-5568. https://doi.org/10.1039/C0DT01601B

Tan ZF, Li JH, Zhang C, et al., 2018. Highly efficient blue-emitting Bi-doped Cs_2SnCl_6 perovskite variant: photoluminescence induced by impurity doping. *Advanced Functional Materials*, 28(29):1801131. https://doi.org/10.1002/adfm.201801131

Tan ZK, Moghaddam RS, Lai ML, et al., 2014. Bright light-emitting diodes based on organometal halide perovskite. *Nature Nanotechnology*, 9(9):687-692. https://doi.org/10.1038/nnano.2014.149

Tang WD, Liu SN, Zhang G, et al., 2025. Lead-free perovskite light-emitting diodes. *Advanced Materials*, 37(25):2411020. https://doi.org/10.1002/adma.202411020

Todorović P, Ma DX, Chen B, et al., 2019. Spectrally tunable and stable electroluminescence enabled by rubidium doping of $CsPbBr_3$ nanocrystals. *Advanced Optical Materials*, 7(24):1901440. https://doi.org/10.1002/adom.201901440

Tong YF, Bi XY, Xu S, et al., 2023. In situ halide exchange of cesium lead halide perovskites for blue light-emitting diodes. *Advanced Materials*, 35(3):2207111. https://doi.org/10.1002/adma.202207111

van der Stam W, Geuchies JJ, Altantzis T, et al., 2017. Highly emissive divalent-ion-doped colloidal $CsPb_{1-x}M_xBr_3$ perovskite nanocrystals through cation exchange. *Journal of the American Chemical Society*, 139(11):4087-4097. https://doi.org/10.1021/jacs.6b13079

Wang K, Jin LR, Gao Y, et al., 2021. Lead-free organic–perovskite hybrid quantum wells for highly stable light-emitting diodes. *ACS Nano*, 15(4):6316-6325. https://doi.org/10.1021/acsnano.1c00872

Wang LT, Shi ZF, Ma ZZ, et al., 2020. Colloidal synthesis of ternary copper halide nanocrystals for high-efficiency deep-blue light-emitting diodes with a half-lifetime above 100 h. *Nano Letters*, 20(5):3568-3576. https://doi.org/10.1021/acs.nanolett.0c00513

Wang TY, Zhou DL, Wang YQ, et al., 2025. Lanthanide-based lead-free perovskite materials for visible-range and infrared light-emitting diodes. *Advanced Functional Materials*, 35(33):2504436. https://doi.org/10.1002/adfm.202504436

Wei S, Han X, Zhang K, et al., 2026. Stable energy-level regulation of NiO_x for efficient deep-blue perovskite LEDs. *Advanced Materials*, 38(36):e73478. https://doi.org/10.1002/adma.73478

Whitehead CB, Özkar S, Finke RG, 2019. LaMer's 1950 model for particle formation of instantaneous nucleation and diffusion-controlled growth: a historical look at the model's origins, assumptions, equations, and underlying sulfur sol formation kinetics data. *Chemistry of Materials*, 31(18):7116-7132. https://doi.org/10.1021/acs.chemmater.9b01273

Wong AB, Bekenstein Y, Kang J, et al., 2018. Strongly quantum confined colloidal cesium tin iodide perovskite nanoplates: lessons for reducing defect density and improving stability.

Nano Letters, 18(3):2060-2066. https://doi.org/10.1021/acs.nanolett.8b00077

Wu YQ, Yang SZ, Li EL, et al., 2025. Low-dimensional templates and delayed crystallization for high-quality tin-based perovskite films and high-performance transistors. *Nature Communications*, 16(1):9505. https://doi.org/10.1038/s41467-025-64560-2

Xia ML, Yuan JH, Niu GD, et al., 2020. Unveiling the structural descriptor of $A_3B_2X_9$ perovskite derivatives toward X-ray detectors with low detection limit and high stability. *Advanced Functional Materials*, 30(24):1910648. https://doi.org/10.1002/adfm.201910648

Xia Y, Song B, Zhang ZP, et al., 2024. Vertically concentrated quantum wells enabling highly efficient deep-blue perovskite light-emitting diodes. *Angewandte Chemie International Edition*, 63(22):e202403739. https://doi.org/10.1002/anie.202403739

Xing GC, Mathews N, Lim SS, et al., 2014. Low-temperature solution-processed wavelength-tunable perovskites for lasing. *Nature Materials*, 13(5):476-480. https://doi.org/10.1038/nmat3911

Xu B, Yuan SC, Wang LQ, et al., 2025. Highly efficient blue light-emitting diodes enabled by gradient core/shell-structured perovskite quantum dots. *ACS Nano*, 19(3):3694-3704. https://doi.org/10.1021/acsnano.4c14276

Yang XY, Ma L, Yu MT, et al., 2023. Focus on perovskite emitters in blue light-emitting diodes. *Light: Science & Applications*, 12(1):177. https://doi.org/10.1038/s41377-023-01206-2

Yao JY, Liu H, Chen ZN, et al., 2025. Low-dimensional lead-free metal halides for efficient electrically driven light-emitting diodes. *Angewandte Chemie International Edition*, 64(6):e202423185. https://doi.org/10.1002/anie.202423185

Yu MB, Qin TX, Gao G, et al., 2025. Multiple defects renovation and phase reconstruction of reduced-dimensional perovskites via in situ chlorination for efficient deep-blue (454 nm) light-emitting diodes. *Light: Science & Applications*, 14(1):102. https://doi.org/10.1038/s41377-025-01768-3

Yuan S, Wang ZK, Xiao LX, et al., 2019. Optimization of low-dimensional components of quasi-2D Perovskite films for deep-blue light-emitting diodes. *Advanced Materials*, 31(44):1904319. https://doi.org/10.1002/adma.201904319

Yuan S, Dai LJ, Sun YQ, et al., 2024. Efficient blue electroluminescence from reduced-dimensional perovskites. *Nature Photonics*, 18(5):425-431. https://doi.org/10.1038/s41566-024-01382-6

Yuan Z, Shu Y, Xin Y, et al., 2016. Highly luminescent nanoscale quasi-2D layered lead bromide perovskites with tunable emissions. *Chemical Communications*, 52(20):3887-3890. https://doi.org/10.1039/C5CC09762B

Zeng MX, Chen D, Wang JJ, et al., 2023. Deep-blue perovskite light-emitting diodes realized by a dynamic interfacial ion exchange. *ACS Applied Materials & Interfaces*, 15(30):36620-36627. https://doi.org/10.1021/acsami.3c05253

Zhang F, Zhao ZH, Chen BK, et al., 2020. Strongly emissive lead-free 0D $Cs_3Cu_2I_5$ perovskites synthesized by a room temperature solvent evaporation crystallization for down-conversion light-emitting devices and fluorescent inks. *Advanced Optical Materials*, 8(8):1901723. https://doi.org/10.1002/adom.201901723

Zhang K, Shen Y, Cao LX, et al., 2024. Nondestructive halide exchange via S_N2-like mechanism for efficient blue perovskite light-emitting diodes. *Nature Communications*, 15(1):10621. https://doi.org/10.1038/s41467-024-55074-4

Zhang L, Long R, 2022. Developments and challenges ahead in blue perovskite light-emitting devices. *Journal of Energy Chemistry*, 71:418-433. https://doi.org/10.1016/j.jechem.2022.04.001

Zhang XT, Wang CC, Zhang Y, et al., 2019. Bright orange electroluminescence from lead-free two-dimensional perovskites. *ACS Energy Letters*, 4(1):242-248. https://doi.org/10.1021/acsenergylett.8b02239

Zhao BD, Vasilopoulou M, Fakharuddin A, et al., 2023. Light management for perovskite light-emitting diodes. *Nature Nanotechnology*, 18(9):981-992. https://doi.org/10.1038/s41565-023-01482-4

Zhao BD, Guo BB, Xing SY, et al., 2024. Highly stable perovskite light-emitting diodes. *Matter*, 7(3):772-793. https://doi.org/10.1016/j.matt.2023.11.022

Zhao JP, Han BN, Wang JH, et al., 2024. Blue lead-free perovskite derivatives: structural diversity, luminescence properties and light-emitting diode applications. *Advanced Optical Materials*, 12(19):2400277. https://doi.org/10.1002/adom.202400277

Zhao SH, Yu H, Jia YH, et al., 2024. Postdeposition halide exchange for achieving deep-blue perovskite light-emitting diodes: the role of the organic cations in the chloride source. *Small Methods*, 8(2):2300572. https://doi.org/10.1002/smtd.202300572

Zheng XP, Yuan S, Liu JK, et al., 2020. Chlorine vacancy passivation in mixed halide perovskite quantum dots by organic pseudohalides enables efficient Rec. 2020 blue light-emitting diodes. *ACS Energy Letters*, 5(3):793-798. https://doi.org/10.1021/acsenergylett.0c00057

Zhu YS, Zhu JY, Song HZ, et al., 2021. Samarium doping improves luminescence efficiency of $Cs_3Bi_2Br_9$ perovskite quantum dots enabling efficient white light-emitting diodes. *Journal of Rare Earths*, 39(4):374-379. https://doi.org/10.1016/j.jre.2020.06.007

Zou C, Liu Y, Ginger DS, et al., 2020. Suppressing efficiency roll-off at high current densities for ultra-bright green perovskite light-emitting diodes. *ACS Nano*, 14(5):6076-6086. https://doi.org/10.1021/acsnano.0c01817